Coadministration of Vascular Disrupting Agents and Nanomedicines to Eradicate Tumors from Peripheral and Central Regions

Wantong Song, Zhaohui Tang, Dawei Zhang, Haiyang Yu, and Xuesi Chen**

Nanosized anticancer drug delivery systems hold great promise for safe, simple, and effective therapies against malignant solid tumors.[1–5] Nanoparticles accumulate in solid tumors by virtue of size and longevity in blood circulation due to the enhanced permeability and retention (EPR) effect.[6,7] This phenomenon was reported by Maeda and Matsumura in the mid-1980s and has since been confirmed by a flood of preclinical studies of drug-loaded nanoparticles.[8] Currently, more than ten nanocarrier-based drugs have been marketed for the treatment of cancer since the mid-1990s.[9,10] However, these nanocarrier-based drugs have only offered modest overall clinical benefits. In particular, drugs delivered by nanocarrier systems generally fail to provide superior efficacy to free drug systems in clinical trials. For example, pegylated liposomal doxorubicin (Doxil) is a typical nanocarrier-based drug that did not show improved efficacy in the treatment of solid tumors when compared to standard therapies, although it did enhance accumulation of doxorubicin within the tumor. This may be explained by the presence of permeability barriers within the central region of solid tumors, which results in a low contact probability for the drug-loaded nanoparticles to reach a majority of the targeted cells.[11–15]

The penetration of nanoparticles is poor in solid tumor tissues.[16,17] Studies have indicated that most stealth liposomes are located within 30 μm of the tumor vessel wall at about one week following tail vein injection.[18] Furthermore, the traveling distance of block copolymer micelles in a solid tumor is extremely limited (42 μm) even when the size of the micelles is relatively small (25 nm).[19] Liang and co-workers reported that gold-coated nanoparticles with a diameter of 100 nm were primarily localized in the periphery of the tumor spheroid and around blood vessels, hindering deep penetration into the tumors.[20] Although the tumor accumulation and distribution of nanoparticles can be mediated by virtue of size or surface chemistry, most injected nanoparticles are still distributed in the perivascular regions of solid tumors.[6,21] As such, drug-loaded nanoparticles are generally able to reach the cancer cells in the tumor periphery, but leave most tumor cells in the central regions unaffected due to the decreased vascularization of the central region compared to the periphery.[22–24] This, in turn, limits the efficacy of drug-loaded nanoparticles against solid tumor cancers. Therefore, in order to improve the therapeutic efficacy of nanocarrier-based drugs, a strategy that can eradicate tumor cells in both the central and peripheral regions of a solid tumor is highly desired.

Recently, small-molecule vascular disrupting agents (VDAs) have been shown to cause a pronounced shutdown in blood flow to solid tumors, resulting in extensive necrosis selectively in the tumor center. Furthermore, the blood flow in normal tissues is left relatively intact following treatment.[25–30] Therefore, small-molecule VDAs have great potential to overcome the failure of nanocarrier-based drugs to kill the cells within the central regions of solid tumors. VDAs have been extensively studied in combination therapy of cancer treatment.[31–34] In particular, Sengupta et al.[35] reported a nanoscale codelivery system of combretastatin A4 (CA4) and doxorubicin for tumor therapy. The system enabled focal sequential release of CA4 and doxorubicin within a solid tumor, and resulted in improved therapeutic index with reduced toxicity. This revealed the advantage of focal sequential release of VDAs and chemotherapeutic agents for solid tumor therapy. However, to the best of our knowledge, free small-molecule VDAs have never been reported to make up the shortcoming of nanocarrier-based drugs for the treatment of tumor cells in the central regions.

As a typical small-molecule VDA, combretastatin A4 disodium phosphate (CA4P) is a prodrug of CA4, and is currently in phase I/II clinical trials for the treatment of solid tumors.[36,37] After administration, CA4 is released from CA4P and binds to tubulin, which destabilizes the tubulin polymers of the cytoskeleton. This, in turn, leads to rapid morphological changes of the endothelial cells and increased vascular permeability.[38,39] Clearly, if rapid changes in endothelial cell morphology and detachment occur in vivo, exposure of the basement membrane and a physical narrowing of the vessel lumen will contribute to the reduction in capillary blood flow, increasing vascular resistance as well as inducing hemorrhage, coagulation, and vessel occlusion.[31] Thus, all downstream cells supplied by those vessels are killed. Free CA4P typically produces massive necrosis within

Dr. W. Song, Dr. Z. Tang, D. Zhang, H. Yu, Prof. X. Chen
Key Laboratory of Polymer Ecomaterials
Changchun Institute of Applied Chemistry
Chinese Academy of Sciences
Changchun 130022, P. R. China
E-mail: ztang@ciac.ac.cn; xschen@ciac.ac.cn

DOI: 10.1002/smll.201500324

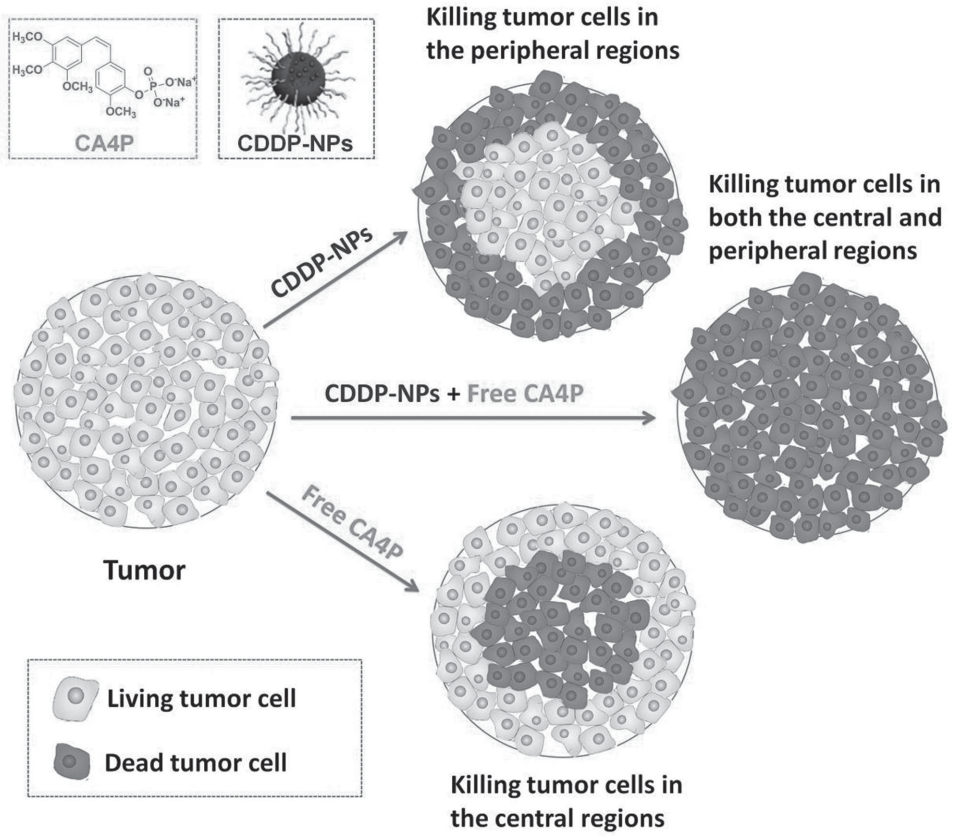

Figure 1. Schematic representation of the mechanism of coadministration of CDDP-NPs plus CA4P. CDDP-NPs mainly act on the tumor periphery, while leaving the central regions unaffected. CA4P eradicates tumor cells in the central regions of a solid tumor. In contrast, the coadministration of CDDP-NPs plus CA4P results in the eradication of the entire tumor.

a tumor center; however, peripheral cells around the tumor survive as they are able to receive sufficient oxygen and nutrients to maintain viability through diffusion from vessels in the surrounding normal tissues.[40] Therefore, the coadministration of free CA4P and nanocarrier-based drugs may provide a complementary effect that is absent when either drug is administered alone. In particular, free CA4P has the potential to overcome the failure of nanocarrier-based drugs to kill the cancer cells within the tumor centers.

Studies have shown that free CA4P selectively targets endothelial cells by disrupting their cell-to-cell interactions that are mediated by the vascular endothelial cadherin/β-catenin complex. The disruption of this adhesive interaction is inhibited by the presence of smooth muscle cells, which are typically present in normal tissue vasculature.[41] Consequently, the tumor specificity of CA4P is believed to be due to its targeting of recently formed endothelial cells in immature or abnormal vessels which lack a full complement of smooth muscle cells or pericyte support.[40] In addition, the tumor specificity of CA4P may be due to other characteristics of the tumor microcirculation, such as high interstitial fluid pressure, procoagulant status, vessel tortuosity, and heterogeneous blood flow distribution.[42,43]

Previously, we reported *cis*-diamminedichloroplatinum (CDDP) loaded nanoparticles (CDDP-NPs) prepared from CDDP and poly(l-glutamic acid)-*g*-methoxy poly(ethylene glycol) (PLG-*g*-mPEG) (Figure S1, Supporting Information).[44] The CDDP-NPs have significantly longer blood retention time and improved tumor accumulation, along with lower systemic toxicity when compared with free CDDP.[44] However, the treatment with CDDP-NPs does not result in improved antitumor efficacy when compared to free CDDP. In this study, we demonstrated that the coadministration of free CA4P plus CDDP-NPs would make up for the low efficacy of CDDP-NPs by eradicating tumor cells in both the central and peripheral regions (**Figure 1**).

We first investigated the intratumor distribution of CDDP-NPs. Multispectral optoacoustic tomography (MSOT), which can give whole-body visualization of molecular markers in small animals, was applied.[45,46] CDDP-NPs were labeled with IR830, a near-infrared dye with maximal absorption at 815 nm in water (Scheme S1, Figure S2A, Supporting Information), and injected into Balb/C nude mice bearing MDA-MB-435 tumors. As shown in **Figure 2**A, IR830-labeled CDDP-NPs mainly localized in the tumor periphery, but were rare in the tumor central regions. The hemoglobin/oxyhemoglobin (Hb/HbO_2) images from MSOT reflect the location of blood vessels inside the tumor (Figure S3, Supporting Information), and one can see that the periphery of the MDA-MB-435 tumor is well vascularized, while the central regions are less vascularized. These results suggest that the distribution of CDDP-NPs is vascular-dependent and further explains the low penetration observed in the tumor tissue; injected nanoparticles are restricted to areas near the blood vessels in

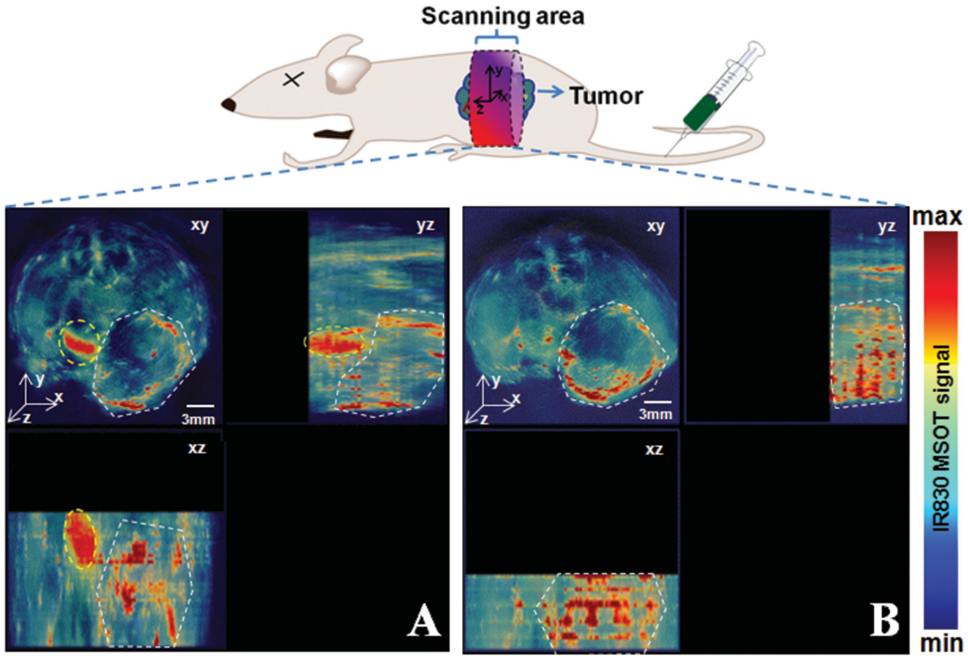

Figure 2. Orthogonal views of MSOT images of MDA-MB-435 tumor–bearing mice at 4 h after injection of IR830-labeled CDDP-NPs A) without or B) with CA4P (100 mg kg^{-1}). The 3D coordinate system defines the orientations and positions of the orthogonal views. The regions circled with dashed yellow and white lines are bladder and tumor regions, respectively.

the tumor periphery. CA4P induces obvious hemorrhage to MDA-MB-435 tumors at dosage over 100 mg kg^{-1} (Figure S4, Supporting Information). When IR830-labeled CDDP-NPs were coadministrated with free CA4P at 100 mg kg^{-1}, similar results were obtained, that is, the nanoparticles were primarily dispersed at the tumor periphery with abundant vessels (Figure 2B and Figure S5, Supporting Information). These indicated that CDDP-NPs could only kill the tumor cells near blood vessels in the tumor periphery, but leave many tumor cells in the central regions survival.

CDDP-NPs are primarily localized in the tumor periphery, which was further confirmed by histopathological analysis. Rhodamine B-labeled CDDP-loaded nanoparticles (RhoB-labeled CDDP-NPs, Scheme S2, Figure S2B, Supporting Information) were administered into Balb/C mice bearing murine colon C26 tumors. Mice were sacrificed 4 and 24 h postadministration and tumors were collected, frozen, sectioned, and stained with fluorescein isothiocyanate (FITC)-labeled goat anti-rabbit immunoglobulin G (IgG) CD31 antibody for visualization of the tumor vasculature. 4′,6-diamidino-2-phenylindole (DAPI) was used to show the cell nuclei. As shown in **Figure 3**, RhoB fluorescence for the RhoB-labeled CDDP-NPs treated group was primarily colocalized with the FITC fluorescence at both 4 and 24 h, indicating that RhoB-labeled CDDP-NPs were primarily localized in the vicinity of blood vessels. Moreover, both FITC and RhoB signals at the tumor periphery were much stronger than those at the central regions, suggesting that blood vessels and nanoparticles were mainly distributed at the peripheral regions of the treated tumors. These results suggest that CDDP-NPs alone do not efficiently kill cancer cells within the tumor center. Similar results were observed in the case of RhoB-labeled CDDP-NPs + CA4P (Figure S6, Supporting Information) though the injection of 100 mg kg^{-1} CA4P caused macroscopical hemorrhage to C26 tumors (Figure S7, Supporting Information). These are consistent with those observed by MSOT.

Next, we compared the effects of CA4P, CDDP-NPs, and CDDP-NPs + CA4P on tumor necrosis after a single intravenous injection by hematoxylin and eosin staining (H&E stain). As shown in **Figure 4**A, CDDP-NPs only caused partial necrosis in the tumors, leaving large regions of the tumor unaffected. This is consistent with our previous observation that CDDP-NPs can only reach the peripheral regions of the tumor containing a good blood supply. In contrast, CA4P selectively induced significant tumor necrosis in the central region of a treated tumor (Figure 4B), which is consistent with literature reports.[43,47] It is noteworthy that CDDP-NPs + CA4P eradicated tumor cells in both the central and peripheral regions of the MDA-MB-435 tumors (Figure 4C), confirming that coadministration of free CA4P plus CDDP-NPs has the potential to eradicate the entire solid tumor, both in the peripheral and central regions. The necrosis rate was 15.0% ± 3.7%, 62.2% ± 8.2%, and 92.8% ± 3.0% for the CDDP-NPs, CA4P, and CDDP-NPs + CA4P group, respectively (Figure 4D), which further demonstrated the advantage of the coadministration of CDDP-NPs plus free CA4P.

Finally, the in vivo anticancer efficacy of CDDP, CDDP-NPs, CA4P, and CDDP-NPs + CA4P was investigated in C26 tumor–bearing Balb/C mice and MDA-MB-435 tumor–bearing Balb/C nude mice. Mice were randomly divided into five groups and then treated with saline, CDDP (4 mg kg^{-1}), CDDP-NPs (4 mg CDDP equivalent kg^{-1}), CA4P (100 mg kg^{-1}), and CDDP-NPs (4 mg CDDP equivalent kg^{-1}) + CA4P (100 mg kg^{-1}) by intravenous injection. The

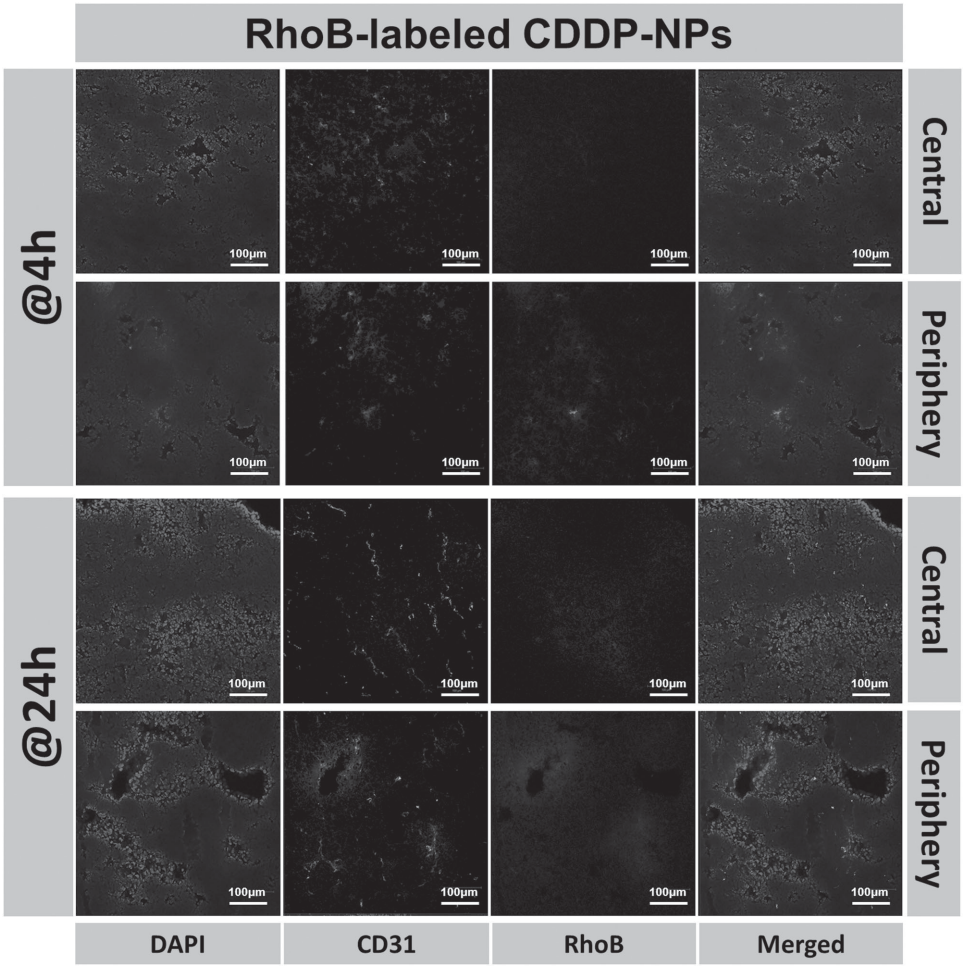

Figure 3. Histopathological analyses of C26 tumors at 4 and 24 h after injection. The tumor center and periphery are shown separately (scale bars = 100 μm).

treatments for C26 tumors were carried out at day 1, 3, and 8, and the tumor volumes and body weights were recorded for 12 d. As shown in **Figure 5**A,B, the tumor suppression rate (TSR) of CDDP, CDDP-NPs, CA4P, and CDDP-NPs + CA4P groups was 76.3%, 68.2%, 54.7%, and 87.5%, respectively. The CDDP group exhibited significant tumor growth suppression; however, this was concurrent with a severe loss of body weight. In comparison, CDDP-NPs are relatively safe compared to free CDDP at the same dosage, however the tumor therapeutic efficacy is modest and lower than CDDP alone. Similarly, the use of free CA4P as a single therapeutic agent is not a very effective treatment method, due to the limited inhibition on tumor volume growth. It is noteworthy that the coadministration of CDDP-NPs plus free CA4P showed the highest tumor inhibition effect without significant body weight loss of all the treatments studied. Tumor growth rate was significantly reduced from 1 to 10 d after coadministration of free CA4P and CDDP-NPs, though rapid tumor regrowth inevitably happened at the later stage. Similar results were obtained in the MDA-MB-435 xenograft model (Figure 5C,D), which clearly demonstrated that the coadministration of CDDP-NPs plus free CA4P had enhanced antitumor efficacy with reduced toxicity, as compared with free CDDP alone.

In summary, we developed a strategy for coadministering CDDP-NPs plus free small-molecule VDAs in order to improve treatment efficacy within the central region of solid tumors. By utilizing MSOT imaging and histopathological analysis, we demonstrate that the distribution of CDDP-NPs in tumors is highly vascular-dependent, and the CDDP-NPs can only access the peripheral region of the tumors. H&E staining confirms that the coadministration of CDDP-NPs plus free CA4P improves the treatment efficacy in both the central and peripheral regions of a treated solid tumor. Specifically, CDDP-NPs + CA4P results in significantly higher anticancer efficacy in comparison with CDDP-NPs or CA4P alone as shown in in vivo experiments using mouse xenograft models bearing C26 and MDA-MB-435 tumors. These results confirm that coadministration of CDDP-NPs plus free CA4P presents a promising strategy for overcoming the inability of CDDP-NPs to access the central regions of a treated solid tumor. Our work supports the notion that coadministration of nanocarrier-based drugs plus free small-molecule VDAs will serve as a promising

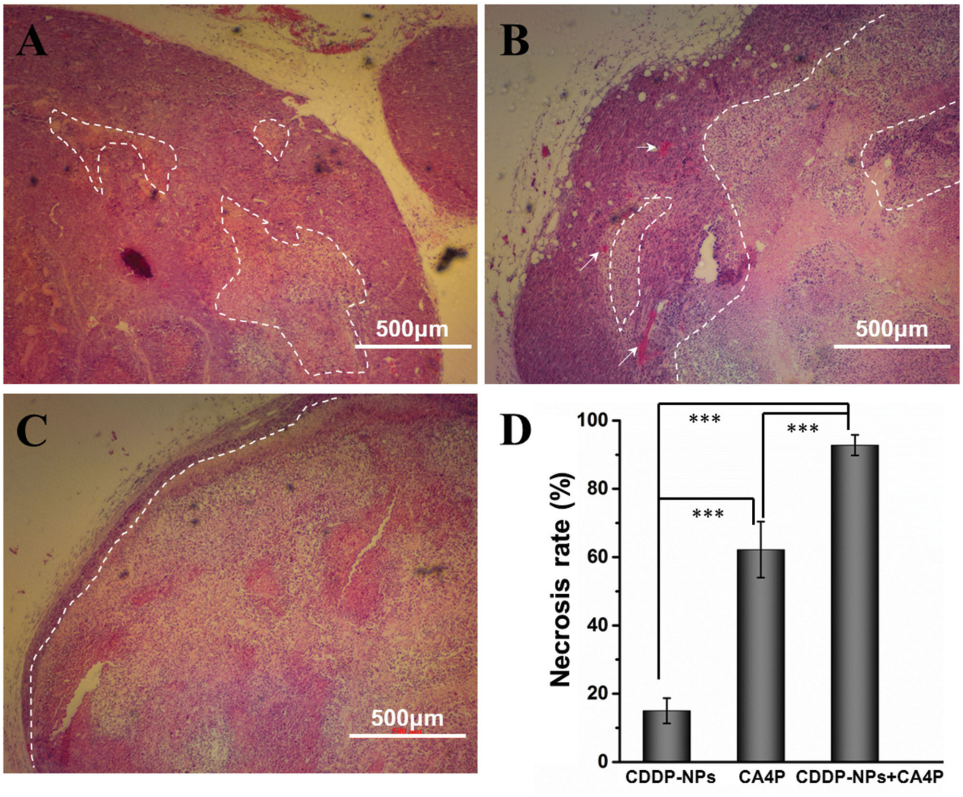

Figure 4. H&E analyses of MDA-MB-435 tumors at 72 h after a single intravenous injection with A) CDDP-NPs (4 mg CDDP equivalent kg^{-1}), B) CA4P (100 mg kg^{-1}), or C) CDDP-NPs (4 mg CDDP equivalent kg^{-1}) + CA4P (100 mg kg^{-1}). The necrotic regions are defined as sections with light color and less cells. The dashed white line indicates the necrotic regions. The red aggregates (labeled with white arrows) in the CA4P group are coagulation regions. D) The necrosis rate is defined as the percentage of necrotic area in given tumor sections ($n = 5$, $^{***}p < 0.001$).

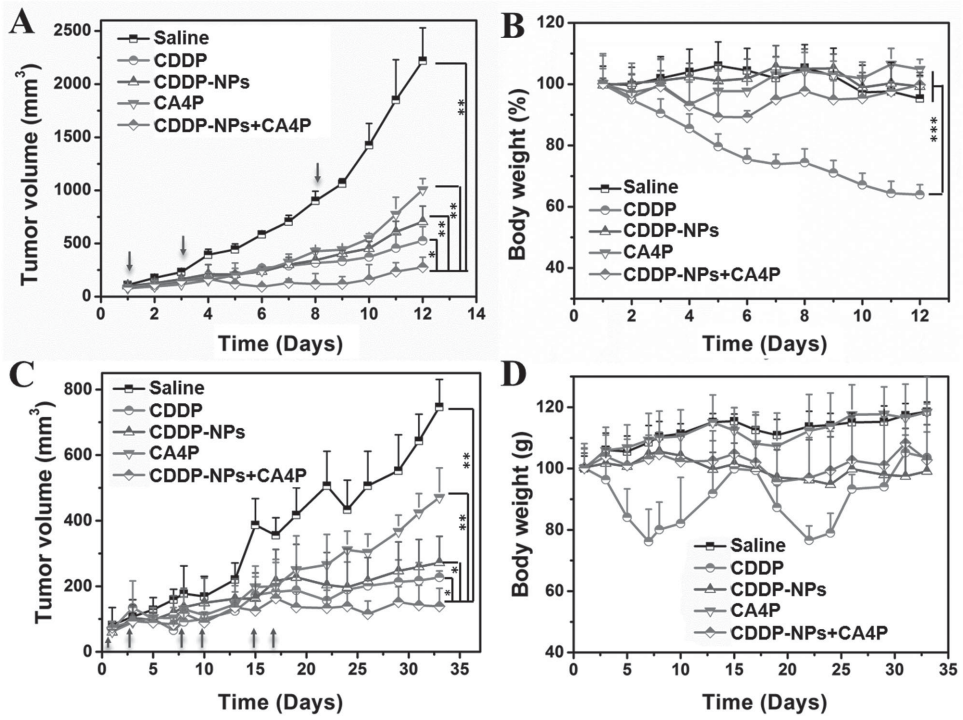

Figure 5. Tumor therapy effect of saline, CDDP (4 mg kg^{-1}), CDDP-NPs (4 mg CDDP equivalent kg^{-1}), CA4P (100 mg kg^{-1}), and CDDP-NPs (4 mg CDDP equivalent kg^{-1}) + CA4P (100 mg kg^{-1}) on A,B) C26 tumor–bearing Balb/C mice and C,D) MDA-MB-435 tumor–bearing Balb/C nude mice. For C26 tumors, the injections were carried out at day 1, 3, and 8. For MDA-MB-435 tumors, injections were carried out at day 1, 3, 8, 10, 15, and 17 except CDDP. Because of severe systemic toxicity, CDDP was only administered at day 1, 3, and 17 ($n = 6$, $^{*}p < 0.05$, $^{**}p < 0.01$, $^{***}p < 0.001$).

strategy for the treatment of solid tumors with high efficacy and low side effects.

Experimental Section

CDDP-NPs: CDDP-NPs were prepared by complexation of PLG-*g*-mPEG [M_n(GPC) 37.3×10^3 g mol^{-1}, PDI(GPC) 1.91, using polyethylene glycol as the standard] with CDDP as a procedure that is reported elsewhere.[44] The CDDP loading content, hydrodynamic radius (R_h), and zeta potential were 19.5 wt%, 12.1 ± 0.9 nm, and −8.5 ± 1.3 mV, respectively. IR830-labeled CDDP-NPs (R_h = 15.1 ± 2.1 nm, zeta potential = −8.1 ± 1.1 mV) or RhoB-labeled CDDP-NPs (R_h = 14.4 ± 1.7 nm, zeta potential = −10.2 ± 0.7 mV) were prepared by a similar procedure to CDDP-NPs using IR830- or RhoB-labeled PLG-*g*-mPEG instead of PLG-*g*-mPEG (Supporting Information).

Animal Use: All the animal experiments were conducted in accordance with the guidelines of the Laboratory Protocol of Animal Care and Use Committee, Jilin University. Balb/C and Balb/C nude mice (5–6 weeks) were bought from Beijing Huafukang Biological Technology Co. Ltd. (HFK Bioscience, Beijing). Murine C26 and human MDA-MB-435 cancer cell lines were bought from Shanghai Bogoo Biotechnology Co. Ltd., China. The C26 xenograft tumor model was prepared by inoculating the right flank of Balb/C mice with 2.0×10^6 C26 cells, which were maintained by i.p. passage in Balb/C mice. The MDA-MB-435 xenograft tumor model was prepared by subcutaneous injection of MDA-MB-435 cells (2.0×10^6) diluted in matrigel (1:1, BD Biosciences) into the mammary fat pads of Balb/C nude mice.

MSOT Testing: Optoacoustic imaging was performed on a MSOT scanner equipped with 128 ultrasound transducer elements (MSOT inVision 128, iThera Medical GmbH, Munich, Germany). Balb/C nude mice bearing MDA-MB-435 tumors (300–400 mm^3) were injected with IR830-labeled CDDP-NPs with or without CA4P (dosage: 100 mg kg^{-1}). After 4 h, the mice were anaesthetized with 2% isoflurane and placed into the MSOT system. Multispectral process scanning (MSP) was performed at 680, 715, 730, 760, 815, 850, and 900 nm. The results were reconstructed in a linear model, and linear regression was used for the multispectral processing.

Immunohistochemical Staining of the Tumor Tissue: Balb/C mice bearing C26 tumors (300–400 mm^3) were injected with RhoB-labeled CDDP-NPs with or without CA4P (dosage: 100 mg kg^{-1}). After 4 and 24 h, the mice were anesthetized and the chests opened. Phosphate buffered saline (PBS) and paraformaldehyde (4% in PBS) were perfused from the left atrium and tumors were collected and embedded in Tissue-Tek OCT embedding medium. Cryogenic slides (5 μm in thickness) were prepared with a freezing microtome (Leica CM 1900) and placed on polylysine-coated glass slides (Wuhan Boster AR1065).

Immunohistochemical staining was carried out following the immunocytochemistry (ICC) protocol developed by Abcam. Specifically, sections were fixed in 4% paraformaldehyde at room temperature for 15 min, washed three times with PBS, and incubated with 1% BSA in phosphate buffered saline Tween-20 (PBST) for 30 min to block unspecific binding of antibodies. Then, the sections were incubated with antibody CD31 (1:50 diluted in 1% BSA in PBST) in a humidified chamber for 1 h at 37 °C, followed by incubation with a secondary antibody (FITC-labeled goat anti-rabbit IgG) in 1% BSA for 1 h at 37 °C in the dark. After extensive washing with PBS, the sections were counterstained with DAPI for 1 min, and then observed under a confocal laser scanning microscope (CLSM, Carl Zeiss LSM 780).

H&E Staining: Balb/C nude mice bearing an MDA-MB-435 tumor (300–400 mm^3) were injected with CDDP-NPs (4 mg CDDP equivalent kg^{-1}), CA4P (100 mg kg^{-1}), or CDDP-NPs (4 mg CDDP equivalent kg^{-1}) + CA4P (100 mg kg^{-1}). The mice were sacrificed at 72 h. After the mice were sacrificed, tumors were collected, embedded with paraffin, and stained with H&E. The histological alterations were observed by microscopy (Nikon TI-S/L100).

Anticancer Efficacy Studies: The anticancer efficacy was evaluated on C26 tumor–bearing Balb/C mice and MDA-MB-435 tumor–bearing Balb/C nude mice following coadministration of CA4P and CDDP-NPs, respectively. The mice were randomly divided into five groups (n = 6) when the tumor volume reached ≈50–70 mm^3, then treated with saline, CDDP (4 mg kg^{-1}), CDDP-NPs (4 mg CDDP equivalent kg^{-1}), CA4P (100 mg kg^{-1}), or CDDP-NPs (4 mg CDDP equivalent kg^{-1}) + CA4P (100 mg kg^{-1}) by intravenous injection. For C26 tumor–bearing mice, the injection was administered at day 1, 3, and 8, and the tumor volume and body weight were recorded for 12 d. For MDA-MB-435 tumor–bearing mice, CDDP was administered at day 1, 3, and 17 due to severe systemic toxicity, while injection for the other groups was administered at day 1, 3, 8, 10, 15, and 17. Tumor volumes and body weights were recorded for 33 d. The estimated volume of tumors and tumor suppression rates were calculated based on the following equation: Tumor volume = $a \times b^2/2$; Tumor suppression rate (TSR,%) = $[(V_c - V_x)/V_c] \times 100\%$, where a and b are the major and minor axes of the tumors measured by caliper. The control group is represented by c, while x represents the treatment group.

Supporting Information

Supporting Information is available from the Wiley Online Library or from the author.

Acknowledgements

This research was financially supported by National Natural Science Foundation of China (Project Nos. 51173184, 51233004, 51373168, 51390484, and 51403204), Ministry of Science and Technology of China (International Cooperation and Communication Program 2011DFR51090), and the Program of Scientific Development of Jilin Province (20130206058GX and 20130521011JH).

[1] D. Liu, C. Poon, K. Lu, C. He, W. Lin, *Nat. Commun.* **2014**, *5*, 5182.
[2] S. H. Voon, L. V. Kiew, H. B. Lee, S. H. Lim, M. I. Noordin, A. Kamkaew, K. Burgess, L. Y. Chung, *Small* **2014**, *10*, 4993.
[3] Y. Cheng, Q. Dai, R. A. Morshed, X. Fan, M. L. Wegscheid, D. A. Wainwright, Y. Han, L. Zhang, B. Auffinger, A. L. Tobias, E. Rincón, B. Thaci, A. U. Ahmed, P. C. Warnke, C. He, M. S. Lesniak, *Small* **2014**, *10*, 5137.

[4] W. Chen, Y. Yuan, D. Cheng, J. Chen, L. Wang, X. Shuai, *Small* **2014**, *10*, 2678.
[5] F. Chen, W. Cai, *Small* **2014**, *10*, 1887.
[6] E. A. Sykes, J. Chen, G. Zheng, W. C. W. Chan, *ACS Nano* **2014**, *8*, 5696.
[7] M. E. Davis, Z. Chen, D. M. Shin, *Nat. Rev. Drug Discovery* **2008**, *7*, 771.
[8] Y. Matsumura, H. Maeda, *Cancer Res.* **1986**, *46*, 6387.
[9] D. Peer, J. M. Karp, S. Hong, O. C. Farokhzad, R. Margalit, R. Langer, *Nat. Nanotechnol.* **2007**, *2*, 751.
[10] Y. Matsumura, K. Kataoka, *Cancer Sci.* **2009**, *100*, 572.
[11] D. L. Stirland, J. W. Nichols, S. Miura, Y. H. Bae, *J. Controlled Release* **2013**, *172*, 1045.
[12] M. E. R. O'Brien, N. Wigler, M. Inbar, R. Rosso, E. Grischke, A. Santoro, R. Catane, D. G. Kieback, P. Tomczak, S. P. Ackland, F. Orlandi, L. Mellars, L. Alland, C. Tendler, *Ann. Oncol.* **2004**, *15*, 440.
[13] A. Gabizon, H. Shmeeda, Y. Barenholz, *Clin. Pharmacokinet.* **2003**, *42*, 419.
[14] J. W. Nichols, Y. H. Bae, *J. Controlled Release* **2014**, *190*, 451.
[15] K. Park, *ACS Nano* **2013**, *7*, 7442.
[16] Y. H. Bae, K. Park, *J. Controlled Release* **2011**, *153*, 198.
[17] Q. Sun, X. Sun, X. Ma, Z. Zhou, E. Jin, B. Zhang, Y. Shen, E. A. Van Kirk, W. J. Murdoch, J. R. Lott, T. P. Lodge, M. Radosz, Y. Zhao, *Adv. Mater.* **2014**, *26*, 7615.
[18] F. Yuan, M. Leunig, S. K. Huang, D. A. Berk, D. Papahadjopoulos, R. K. Jain, *Cancer Res.* **1994**, *54*, 3352.
[19] H. Lee, H. Fonge, B. Hoang, R. M. Reilly, C. Allen, *Mol. Pharmaceutics* **2010**, *7*, 1195.
[20] S. Huo, H. Ma, K. Huang, J. Liu, T. Wei, S. Jin, J. Zhang, S. He, X.-J. Liang, *Cancer Res.* **2013**, *73*, 319.
[21] S. D. Perrault, C. Walkey, T. Jennings, H. C. Fischer, W. C. W. Chan, *Nano Lett.* **2009**, *9*, 1909.
[22] J. Holash, S. J. Wiegand, G. D. Yancopoulos, *Oncogene* **1999**, *18*, 5356.
[23] J. R. Less, T. C. Skalak, E. M. Sevick, R. K. Jain, *Cancer Res.* **1991**, *51*, 265.
[24] B. A. Graff, I. C. Benjaminsen, K. G. Brurberg, E. B. M. Ruud, E. K. Rofstad, *J. Magn. Reson. Imaging* **2005**, *21*, 272.
[25] G. M. Tozer, C. Kanthou, B. C. Baguley, *Nat. Rev. Cancer* **2005**, *5*, 423.
[26] P. LoRusso, S. Gadgeel, A. Wozniak, A. Barge, H. Jones, Z. DelProposto, P. DeLuca, J. Evelhoch, S. Boerner, C. Wheeler, *Invest. New Drugs* **2008**, *26*, 159.
[27] M. Head, M. B. Jameson, *Expert Opin. Invest. Drugs* **2010**, *19*, 295.
[28] H. C. Ma, C. L. He, Y. L. Cheng, D. S. Li, Y. B. Gong, J. G. Liu, H. Y. Tian, X. S. Chen, *Biomaterials* **2014**, *35*, 8723.
[29] C. Sessa, P. Lorusso, A. Tolcher, F. Farace, N. Lassau, A. Delmonte, A. Braghetti, R. Bahleda, P. Cohen, M. Hospitel, C. Veyrat-Follet, J.-C. Soria, *Clin. Cancer Res.* **2013**, *19*, 4832.
[30] A. K. Nowak, C. Brown, M. J. Millward, J. Creaney, M. J. Byrne, B. Hughes, G. Kremmidiotis, D. C. Bibby, A. F. Leske, P. L. R. Mitchell, N. Pavlakis, M. Boyer, M. R. Stockler, *Lung Cancer* **2013**, *81*, 422.
[31] D. W. Siemann, D. J. Chaplin, P. A. Walicke, *Expert Opin. Invest. Drugs* **2009**, *18*, 189.
[32] F. A. L. M. Eskens, P. Tresca, D. Tosi, L. Van Doorn, H. Fontaine, A. Van der Gaast, C. Veyrat-Follet, C. Oprea, M. Hospitel, V. Dieras, *Br. J. Cancer* **2014**, *110*, 2170.
[33] J. W. Lippert Iii, *Bioorg. Med. Chem.* **2007**, *15*, 605.
[34] M. M. Shenoi, I. Iltis, J. Choi, N. A. Koonce, G. J. Metzger, R. J. Griffin, J. C. Bischof, *Mol. Pharmaceutics* **2013**, *10*, 1683.
[35] S. Sengupta, D. Eavarone, I. Capila, G. Zhao, N. Watson, T. Kiziltepe, R. Sasisekharan, *Nature* **2005**, *436*, 568.
[36] M. Zweifel, G. C. Jayson, N. S. Reed, R. Osborne, B. Hassan, J. Ledermann, G. Shreeves, L. Poupard, S.-P. Lu, J. Balkissoon, D. J. Chaplin, G. J. S. Rustin, Ann. Oncol. **2011**, *22*, 2036.
[37] P. Liu, Y. Qin, L. Wu, S. Yang, N. Li, H. Wang, H. Xu, K. Sun, S. Zhang, X. Han, *Anti-Cancer Drugs* **2014**, *25*, 462.
[38] D. A. Beauregard, S. A. Hill, D. J. Chaplin, K. M. Brindle, *Cancer Res.* **2001**, *61*, 6811.
[39] C. Kanthou, G. M. Tozer, *Blood* **2002**, *99*, 2060.
[40] G. J. Dougherty, D. J. Chaplin, *Vascular Disruptive Agents for the Treatment of Cancer*, Springer, Berlin **2010**, p. 5.
[41] L. Vincent, P. Kermani, L. M. Young, J. Cheng, F. Zhang, K. Shido, G. Lam, H. Bompais-Vincent, Z. Zhu, D. J. Hicklin, *J. Clin. Invest.* **2005**, *115*, 2992.
[42] G. M. Tozer, C. Kanthou, C. S. Parkins, S. A. Hill, *Int. J. Exp. Pathol.* **2002**, *83*, 21.
[43] D. J. Chaplin, S. A. Hill, *Int. J. Radiat. Oncol. Biol. Phys.* **2002**, *54*, 1491.
[44] H. Yu, Z. Tang, D. Zhang, W. Song, Y. Zhang, Y. Yang, Z. Ahmad, X. Chen, *J. Controlled Release* **2014**, *10*, 89.
[45] W. Song, Z. Tang, D. Zhang, N. Burton, W. Driessen, X. Chen, *RSC Adv.* **2015**, *5*, 3807.
[46] A. Taruttis, S. Morscher, N. C. Burton, D. Razansky, V. Ntziachristos, *PLoS One* **2012**, *7*, e30491.
[47] L. Li, A. Rojiani, D. W. Siemann, *Int. J. Radiat. Oncol. Biol. Phys.* **1998**, *42*, 899.

Received: February 2, 2015
Revised: March 24, 2015
Published online: April 28, 2015

